AIP | Journal of Applied Physics

Experimental and theoretical studies on the enhanced photoluminescence activity of zinc sulfide with a capping agent

Yuri V. B. de Santana, Cristiane W. Raubach, Mateus M. Ferrer, Felipe La Porta, Julio R. Sambrano et al.

Citation: J. Appl. Phys. **110**, 123507 (2011); doi: 10.1063/1.3666070
View online: http://dx.doi.org/10.1063/1.3666070
View Table of Contents: http://jap.aip.org/resource/1/JAPIAU/v110/i12
Published by the AIP Publishing LLC.

Experimental and theoretical studies on the enhanced photoluminescence activity of zinc sulfide with a capping agent

Yuri V. B. de Santana,[1,a)] Cristiane W. Raubach,[1] Mateus M. Ferrer,[1] Felipe La Porta,[2] Julio R. Sambrano,[3] Valéria M. Longo,[2] Edson R. Leite,[1] and Elson Longo[2]
[1]*Universidade Federal de São Carlos, INCTMN, 13565-905, São Carlos, SP, Brazil*
[2]*São Paulo State University (UNESP), INCTMN, 14800-900, Araraquara, SP, Brazil*
[3]*Grupo de Modelagem e Simulação Molecular, INCTMN-UNESP, São Paulo State University, 17033-360, Bauru, SP, Brazil*

(Received 13 September 2011; accepted 2 November 2011; published online 20 December 2011)

The photoluminescence (PL) emission from zinc sulfide (ZnS) synthesized by the microwave-assisted solvothermal method in the presence/absence of a capping agent was examined to understand the key role of its PL activity. In addition, we also investigated the electronic structure using a first-principle calculation based on density functional theory (DFT) applied to periodic models at B·LYP level. Two models were selected to simulate the effects of structural deformation on the electronic structure; the ordered o-ZnS model and the disordered d-ZnS model, dislocating the Zn atom, 0.1 Å, in the z-direction. The PLemission in the visible region showed different peak positions and intensities in capped and uncapped ZnS. The PL emission was linked to distinct distortions in lattices and the emission of two colors, green in the capped and blue in the uncapped, was also examined in the light of favorable structural and electronic conditions. The computational simulations indicate that the electronic behavior can be associated with the new electronic levels above the valence band. © *2011 American Institute of Physics*. [doi:10.1063/1.3666070]

I. INTRODUCTION

Semiconductor nanostructures are a class of material that have been extensively investigated due to their significance in fundamental research and their high potential for technological applications.[1] Compound semiconductors such as ZnS, CdS, PbS, ZnSe, etc., are important materials for a variety of applications, and their versatility for their chemical tuning of composition and structure. Zinc sulfide (ZnS) is an important II-VI semiconductor material with a wide bandgap (3.72 eV for the cubic zinc blende phase, and 3.77 eV for the wurtzite phase at 300 K in bulk materials).[2] It has a wide range of applications for flat-panel displays, optical sensors, IR windows, catalysts, lasers, etc.[3–5] Shape and structure are crucial factors in determining the chemical, optical, and electrical properties of these materials.[6,7] Thus, one of the most important goals of modern materials research is the development of simple chemical methods for large scale synthesis of nanomaterials with full control of defects and morphology and, in this context, a considerable variety of methods has been reported for the synthesis of ZnS nanocrystals.[8–14] Some of these methods employ the use of capping agents for the passivation of these nanoscrystals or to activate desired morphologies.[15–17] Several reports in the literature describe the conditions required for PL.[18–21] In this paper, we present a comparative study of an intense and broad PL at room temperature for ZnS nanocrystals synthesized by an efficient microwave-assisted solvothermal method,[22–24] for different times to clarify the roles capping agents play in the enhanced PL activity of ZnS. The origin of the intense PL bands was investigated by electronic structure calculations carried out within the framework of *ab initio* periodic quantum-mechanical techniques. Evolutions of order–disorder in the network former, Zn, and the different colors of PL emission, are also discussed in light of the complex cluster concept.

II. EXPERIMENT

ZnS powders were synthesized by the efficient microwave assisted solvothermal method for different times. The typical procedure is described as follows: 3.67 mmol of anhydrous $ZnCl_2$ was dissolved in 25 ml of ethylene glycol (EG), and subsequently 22.3 mmol of tetramethylammonium hydroxide (TMAH) was added (solution 1); 3.67 mmol of thiourea was separately dissolved into another 25 mL of EG (solution 2). Under vigorous magnetic stirring, solution 2 was then quickly injected into solution 1. The same procedure previously described was conducted without the use of TMAH. In this sequence, the solution was transferred into a Teflon autoclave, which was sealed and placed inside a domestic microwave-solvothermal system (2.45 GHz, maximum power of 800 W). The microwave-solvothermal processing was performed at 413 K for different times (1, 2, and 4 min). The resulting solution was washed with de-ionized water and ethanol several times to neutralize the solution *p*H (≈7), and the precipitates were finally collected and dried at 333 K (24 h).

The powders obtained were characterized by x-ray diffraction (XRD) collected from 10° to 110° in the 2θ range using Cu $K\alpha$ radiation (Rigaku-DMax/2500PC). Morphological characterizations were performed by field emission scanning

a)Electronic mail: yurivbs@gmail.com.

electron microscopy (FEG-SEM) (Supra 35-VP, Carl Zeiss), and transmission electron microscopy (TEM) (Tecnai G2TF20, FEI). Ultraviolet–visible (UV–vis) spectroscopy for the optical reflectance spectra of ZnS powders was taken using Cary 5 G equipment. The PL spectra were collected with a Thermal Jarrel-Ash Monospec monochromator and a Hamamatsu R446 photomultiplier. The 350.7 nm (2.57 eV) exciting wavelength of a krypton ion laser (Coherent Innova) was used with the output of the laser kept at 200 mW. This excitation wavelength was chosen because it is on the order of the calculated band gap of the material and also to minimize the radioactive transitions near the conduction band. All measurements were taken at room temperature.

III. THEORETICAL STUDIES

The thermodynamically stable phase wurtzite (under normal conditions) was studied. It belongs to the space group $P6_3mc$, and each Zn atom is surrounded by four S atoms at the corners of the tetrahedron.

Periodic DFT calculations with the B3LYP hybrid functional,[25] were performed using the CRYSTAL06 computer code,[26] which has been successfully employed for studies of the electronic and structural properties of diverse compounds.[27–30]

The atomic centers have been described by an all electron basis set, Zn_86-411d31 G,[31] for Zn and S_86-311 G* S,[32] atoms.

As a first step, the optimization of the exponents for the outermost sp and d shells was carried out to minimize the total energy of the structure at experimental parameters. The optimized external exponents are $\alpha_{sp}(Zn) = 0.14349998$, $\alpha_d(Zn) = 0.73000001$ and $\alpha_{sp}(S) = 0.38000002$. The Powel algorithm[33] method was used to perform all basis sets of the optimization procedure.

From these optimized exponents, a new optimization procedure of lattice parameters $\boldsymbol{a}$, $\boldsymbol{c}$, and $\boldsymbol{u}$ was performed. The calculated and experimental values (given in parentheses) are $a = 3.83$ (3.84) Å, $c = 6.26$ (6.29) Å, and $u = 0.379$ (0.375). Our results are in good agreement with other theoretical and experimental data.[34]

Two periodic models were built from these optimized parameters to represent the ordered o-ZnS model and the disordered d-ZnS model, dislocating the Zn atom, 0.1 Å, in the z-direction. These models can be useful to represent different degrees of order-disorder in the material, along with the structural defects resulting from Zn displacements.

Band structures were obtained for 80 $\vec{k}$ points along appropriate high-symmetry paths of the adequate Brillouin zone. Diagrams of the density of states (DOS) were calculated for an analysis of the corresponding electronic structure. The XcrysDen program[35] was used for the design of a band structure diagram.

It should be noted that our models are not meant to represent the exact reality of disordered structures but to offer a simple scheme serving to shed light on the effects of structural deformation on the network former and on the electronic structure without completely suppressing the geometry of the cell, which is useful for periodic calculations.

IV. RESULTS AND DISCUSSION

In Fig. 1, XRD patterns revealed that all diffraction peaks of ZnS powders can be indexed to the hexagonal structure in agreement with the respective JCPDS card 67–453.[36] The diffraction peaks are significantly broadened because of the very small crystallite size that is more evident in samples where TMAH is used (Fig. 1(b)). The existence of a cubic ZnS phase from XRD patterns alone cannot be excluded due to the large similarity between the cubic and hexagonal ZnS structures. Thus, these results indicate that ZnS powders processed in a microwave-solvothermal system are crystalline, pure, and ordered at long range. These results are in very good agreement with other experimental studies.[14] Using the following Debye–Scherer formula,[37] the average crystallite size (CS) of the materials was calculated from the full width at half maximum (FWHM) of the diffraction peaks,

$$CS = k\lambda/\beta \cos \theta, \quad (1)$$

where, k = constant, λ = wavelength of the x-rays in nm, β = FWHM of the major peak in radians, as calculated from

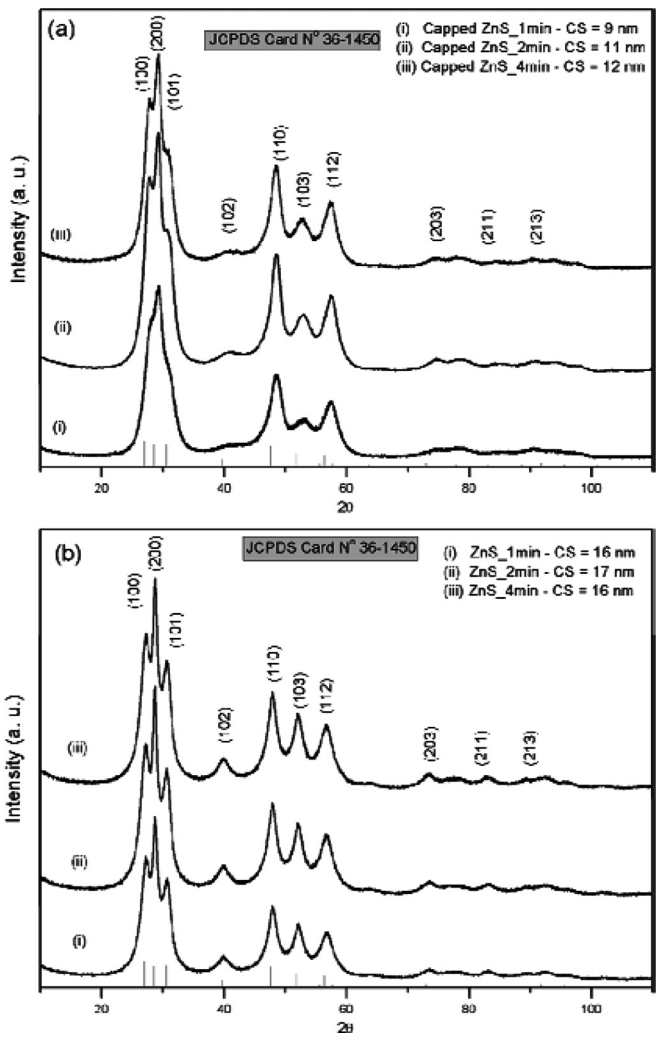

FIG. 1. The XRD patterns of ZnS powders processed in a microwave-solvothermal system at 413 K for different times; (a) capped ZnS, and (b) ZnS. The vertical dashed lines indicate the position and relative intensity of JCPDS card 36-1450.

TABLE I. Comparison among synthesis methods.

Synthesis employed	Reaction time (min)	Temperature (K)
Hydrothermal[a]	300–1320	353–413
Hydrothermal[b]	60–600	433
Solvothermal[c]	5760	443
Solvothermal[d]	720	403–503
Microwave assisted single source method[e]	5	283
This work	1–4	413

[a]Reference 47.
[b]Reference 48.
[c]Reference 49.
[d]Reference 50.
[e]Reference 51.

the data of the XRD peaks, and $\theta =$ diffraction angle. By using the experimental values, the CS was calculated (Fig. 1).

It is important to note that we obtained pure crystalline powders in relatively low temperatures (413 K) in a short time (1 min) which proves the efficiency of the method employed. Table I shows a comparison of other researcher's solvothermal syntheses data, where the wurtzite phase was obtained.

Figures 2 and 3 show FEG-SEM and TEM images for uncapped and capped ZnS nanocrystals, respectively. For uncapped nanocrystals, crystallites agglomerate and form particles with diameters of ~110 nm for a synthesis of 1 min, and there is a greater variation in size with increasing synthesis time (Fig. 2). For capped samples, the crystallites do not show specific morphologies, and form small agglomerates (Fig. 3(a)). In these agglomerates it is difficult to define the crystallites edges and this is because it appears to be amorphous (Fig. 3(b)). Therefore, it is not possible to do a count-statistic on the size of the crystallites. Corresponding FFT images indicated the presence of hexagonal and cubic phases (Figs. 3(d) and 3(c), respectively), as was expected from the XRD diffraction.

Figure 4 shows the absorbance spectral dependence for the processed ZnS powders. The equation proposed by Wood and Tauc[38] was used to estimate the optical bandgap.

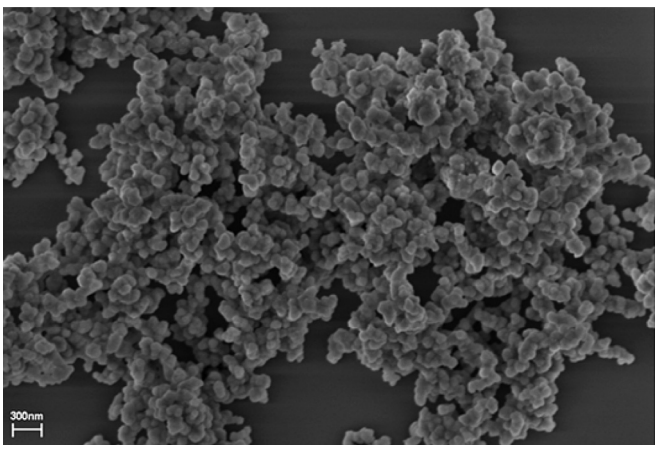

FIG. 2. The FEG-SEM image of 1 min uncapped ZnS.

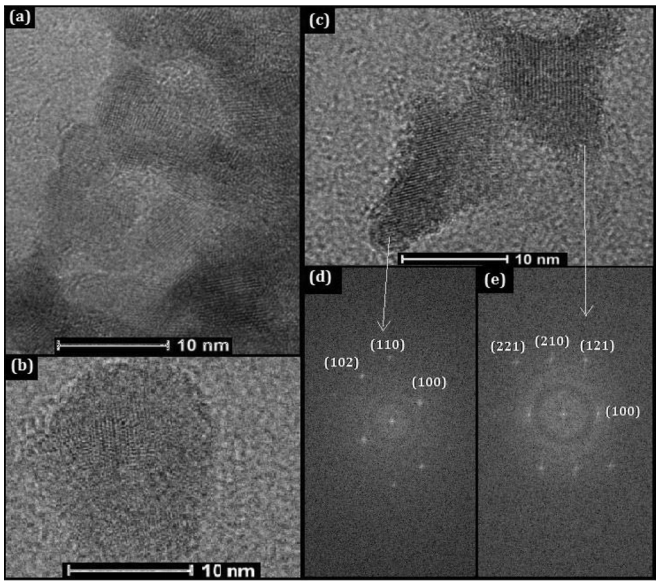

FIG. 3. The FEG-TEM images of 1 min capped ZnS. (a) The crystallites agglomerated, (b) crystallite with amorphous edges, (c) crystallites with cubic and hexagonal phases, (d) hexagonal phase FFT, and (e) cubic phase FFT.

According to these authors, the optical bandgap energy is related to the absorbance and photon energy by Eq. (2),

$$h\upsilon\alpha\ \alpha\ \left(h\upsilon - E_g^{opt}\right)^n, \tag{2}$$

where α is the absorbance, h is Planck's constant, ν is the frequency, Eg is the optical bandgap, and n is a constant associated with the different types of electronic transitions ($n = 1/2$, 2, 3/2, or 3 for direct allowed, indirect allowed, direct forbidden, and indirect forbidden transitions, respectively). The literature[39] reports that the hexagonal ZnS have a typical optical absorption process governed by direct transitions. In fact, considering this information, the Eg values of the ZnS powders were calculated using $n = 2$ in Eq. (2) and extrapolating the linear portion of the curve or tail. The bandgap in the materials is related to the absorbance and photon energy. Therefore, the combination of the absorbance and photoluminescence measurements allows for discovering the energy levels in the materials and the optical bandgap value.

The UV–vis measurements on the six samples showed a typical bandgap value of approximately 3.1 and 3.6 eV for capped and uncapped nanocrystals, respectively (see Fig. 4). The exponential optical absorption edge and hence, the optical bandgap are controlled by the degree of structural order disorder on the ZnS lattice. The decrease in the bandgap can be directly related to the increase in defects in the ZnS lattice; in the present case, dislocations of the network former, Zn, raise the intermediary levels within the bandgap region, reducing the optically measured bandgap. The observed optical bandgap indicates only the presence of defects; hence, localized electronic levels in the forbidden bandgap, nevertheless, do not specifically indicate the structural defects that may be linked to them.

Figure 5 exhibits the PL spectra of capped and uncapped ZnS nanoparticles measured at room temperature and excited at 350.7 nm.

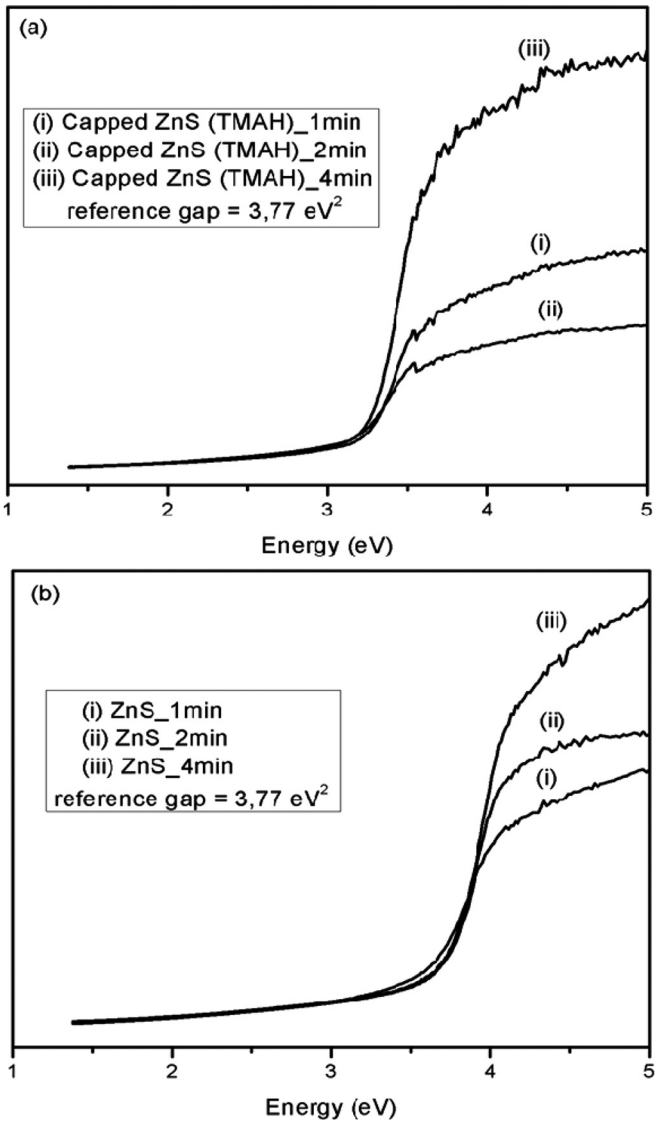

FIG. 4. The UV-vis spectrum of ZnS powders; (a) capped ZnS, and (b) uncapped ZnS.

The profile of the emission band is typical of a multiphonon and multilevel process, i.e., a system in which relaxation occurs by several paths, involving the participation of numerous states within the bandgap of the material. However, the origin of this PL emission has been quite controversial. Kasaii *et al.*[40] attributed the blue emission (~430 and 450 nm) both to Zn and S vacancies. Uchida *et al.*[41] made the correlation with the off stoichiometry of the Zn and S, and concluded that samples with both zinc and sulfur excess emitted in the blue range. Murase *et al.*[42] conducted fluorescence and EPR studies of Mn doped ZnS, and the EPR measurements proved the existence of hole centers, such as Zn vacancies, and attributed the blue emission (~450 nm) to Zn vacancies. Zhang *et al.*[19] attributed the blue emission to defects related to sulfur vacancies. Jun *et al.*[18] associated the blue emission (~479 nm) in ZnS solid nanospheres to Zn vacancies. In addition, in hollow nanospheres they observed a strong green emission band centered at ~509 nm and justified this emission to self-activated centers, vacancy states, or interstitial states associated with that peculiar nanostructure.

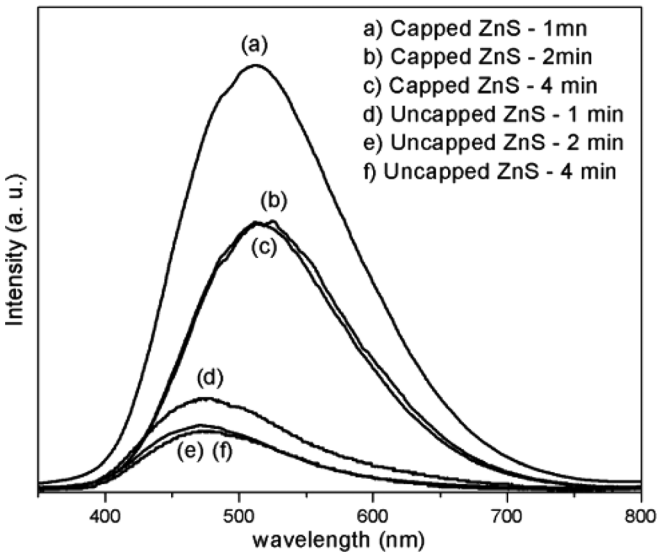

FIG. 5. The PL spectrum of ZnS powders at room temperature.

More recently, Chen *et al.*[43] explained the green emission of the ZnS nanostructures as being due to self-activated zinc vacancy points. Yunchao *et al.*[44] conducted a study comparing the PL of cubic and hexagonal ZnS structures. For cubic ones they attributed the peak at 322 nm to excitonic emission, the peak at 420 nm to Zn or S vacancies, and the 460 nm peak to the trapped surface states emission. For the hexagonal structure, they again attributed the 322 nm peak to excitonic emission, and the peaks at 360 and 375 nm to interstitial sulfur emission and interstitial zinc emission, respectively. Theoretical results have shown that the symmetry break process (an effect of order-disorder) in the structure of various semiconductors is a condition necessary for the existence of intermediary energy levels within the forbidden bandgap.[45] As shown in Figs. 5(a)–5(f), the evolution of the PL spectra was obviously different. During the growth of capped and uncapped ZnS, the peak correlating to the defect states was quenched in the initial 1 min (Figs. 5(a) and 5(d)). However, during the growth process, the peak correlating to the defect states slightly decreased, and remained practically constant during the period from 2 to 4 min (Figs. 5(b), 5(c), 5(e), and 5(f)). The strong defect-induced luminescence of the initial particles could mainly be attributed to the internal lattice defects that arise from the fast deposition during the initial nucleation process. After 2 min, most of the internal defects from the nucleation process had disappeared. Thus, with the size increased, the amount of internal defects and surface defects correspondingly decreased. Since the internal and surface defects are different during different synthetic periods, difficulties arise in the investigation of the relationship between the luminescence properties and the defects states.

This behavior is related to the structural disorder of ZnS and indicates the presence of additional electronic levels in the forbidden bandgap of the material (see Fig. 6). The capped samples presented a maximum emission at 513 nm in the green region of the visible spectra, while the uncapped ones presented a maximum emission at 478 nm in the blue region of the visible spectra. The Stokes shift can be related

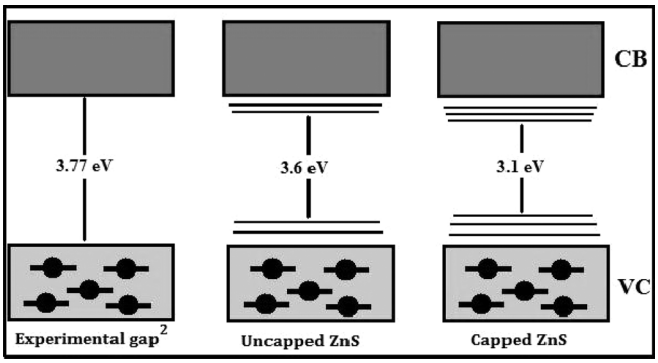

FIG. 6. Wide-band model, indicating the intermediary levels in the forbidden area.

to the difference between the excitation and the emission maximum and represents the strength of the electron-phonon interaction. For the uncapped samples the Stokes shift was 127.3 nm. The capped nanoparticles have a greater Stokes shift of 162.3 nm, indicating a dependence of the electron-phonon interaction on the excitation wavelength and the degree of disorder in the lattice. This rearrangement of the lattice can be attributed to the crystallization process of the capped and uncapped nanoparticles.

Thus, we can understand the materials structures on a length scale. This understanding is relevant in shedding light on several outstanding issues in materials science, clarifying the relationships existing between local, intermediate, and long range structures and the properties of the materials. The theory allied to careful experiments, modeling, and simulations will be required to determine their origins. Experimental probes can provide more structural information on short- and long-range orders in materials; however, their structures over the intermediate range are still little understood. Theoretical calculations and computer simulations can complement experimental methods and have revealed new insights into medium-range order and dynamic changes in the local structure.[46] To understand the relationship between the structural disorder in complex clusters with an intermediate-range interaction (interaction between two clusters) and the resulting electronic defects that are generated, a

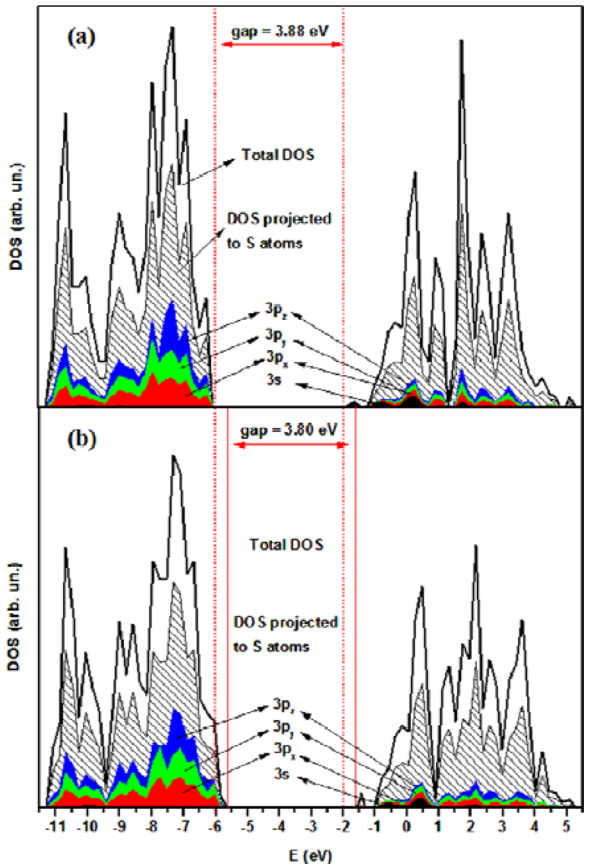

FIG. 8. (Color online) Total and p-DOS calculation on S atoms for (a) o-ZnS, and (b) d-ZnS models.

detailed theoretical study was made of the electronic structure of the ordered o-ZnS model and of the disordered d-ZnS periodic models. To appreciate the differences in the electronic structure, it is important to make reference to quantities such as the band structures and density of states (DOS), which can be compared to each other independent of the crystalline space group.

Figure 7 represents the band structure of the bulk o-ZnS and d-ZnS models. For the o-ZnS and d-ZnS models the top of the valence band (VB), is located at the Γ point. The

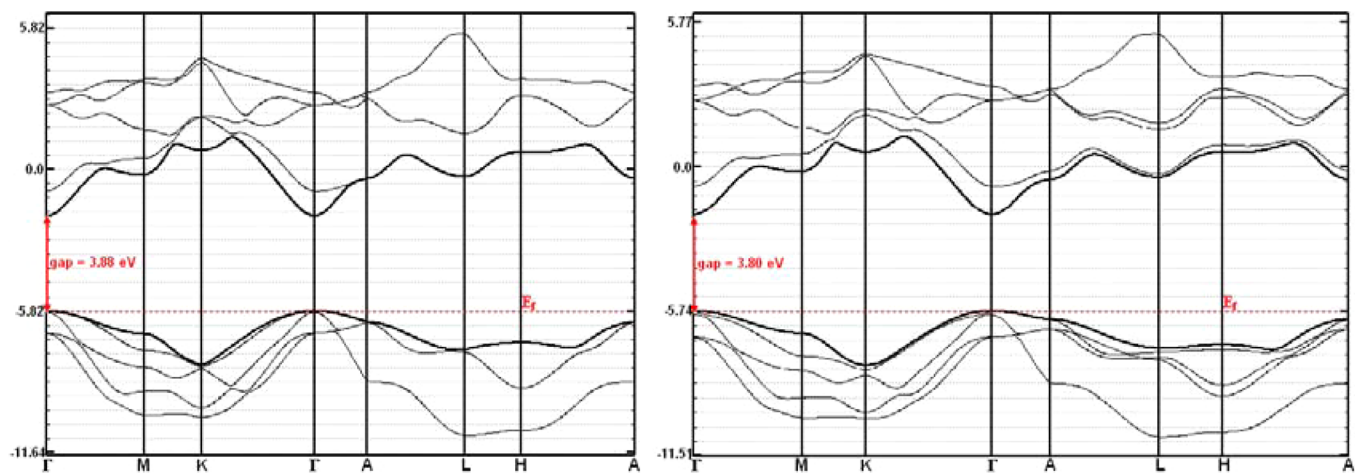

FIG. 7. (Color online) Band structures for (a) o-ZnS, and (b) d-ZnS.

bandgap is direct; 3.88 eV and 3.80 eV, respectively. The calculated bandgap for o-ZnS is in accordance with the experimental optically measured gap (3.77 eV).[2]

An analysis of the projected density of state (DOS-p) for the S atoms of the o-ZnS model, shown in Fig. 8(a), indicate that the VB consists mainly of $3p_x$, $3p_y$, and $3p_z$ levels. The main contribution of conduction band (CB) comes from minor contributions of the 3px, 3py, and 3pz levels with a lower contribution of 3s levels of S atoms. The DOS-p for Zn atoms of the o-ZnS model, shown in Fig. 9(a), show that the VB is made from 4px, 4py, and 4pz orbitals with a minor contribution of 4s levels; the 3d levels have a lower influence. The presence of the 3d states in the VB in the two models reveal a strong bonding character between S and Zn. The same behavior is observed for the CB.

Quantum-mechanical calculations of dislocated ZnS complex clusters indicate that localized states generated in the bandgap reduce the gap energies. When the structural order increases, the gap energy increases. These findings confirm the fact that the PL is directly associated with the localized states existing in the bandgap. Distorted clusters cause local lattice distortion that propagates throughout the material, pushing the surrounding clusters away from their ideal positions. Thus, distorted clusters must move for these properties to occur, changing the electronic distribution along the network of these polar clusters. This electronic structure dictates both optical and electrical transport properties and plays a major role in determining reactivity and stability. However, these movements can be induced within the crystal lattice by the PL measurements and these anisotropic cooperative movements lead to these properties.

The bandgap of capped ZnS is comparatively smaller than that of uncapped ZnS. Therefore, the excitation wavelength of 350.7 nm is able to excite different populations of electrons in the bandgap of the two structures. Here, each color represents a different type of electronic transition and is linked to a specific structural arrangement. In the case of capped ZnS, the recombination of electrons and holes gives rise to a strong green light emission and in the case of uncapped ZnS, to blue light emission. In our model, the wide-band model,[45] the most important events occur before excitation, i.e., before the photon arrives. The deep and shallow defects generated by the complex clusters give rise to localized states in the bandgap and inhomogeneous charge distribution in the cell, allowing electrons to become trapped. The localized levels are energetically distributed so that various energies are able to excite the trapped electrons. These structural changes can be related to the charge polarization

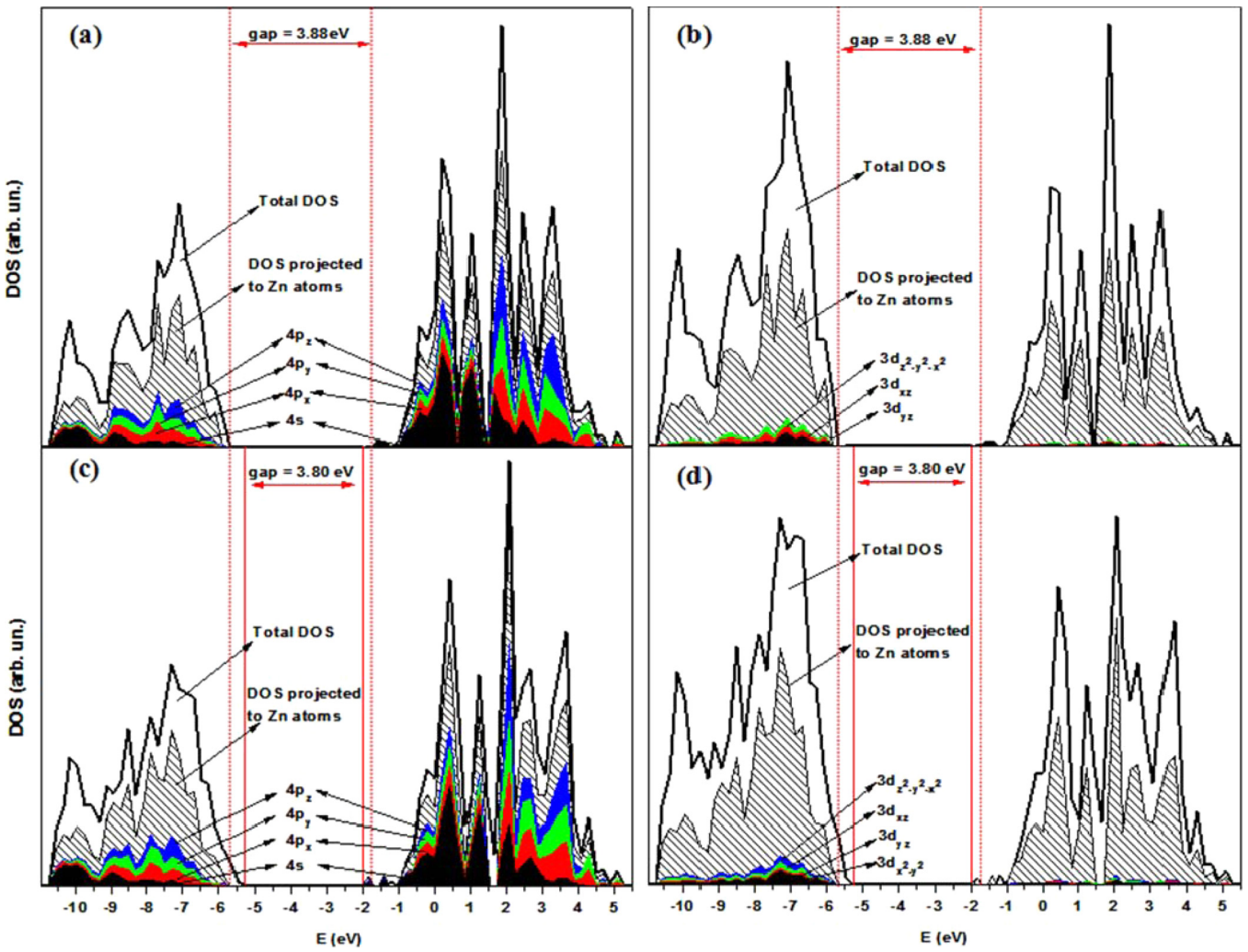

FIG. 9. (Color online) Total and p-DOS calculation on Zn atoms for (a) and (b) o-ZnS, and (c) and (d) d-ZnS models.

in different ranges that are, at least, a manifestation of the quantum confinement, when they occur at short and intermediate range independent of the particle size.

In this paper, we have shown that distinct structures and different orders/disorders in the lattice produce different types of PL emission. The complex clusters already existing in the ground state facilitate the emission process and lead to PL, i.e., radiative recombination. Thus, the distortions of complex clusters are crucial for an understanding of the properties of materials. The study presented here offers a conceptual framework to understand, discuss, and optimize electronic material properties on the basis of their lattice distortions. However, the mechanistic pathway of the PL emission is still not completely understood. Understanding it may provide information about how clustered molecules ''communicate'' with one another in physical and chemical processes.

V. CONCLUSION

The ZnS nanoparticles were successfully synthesized by the microwave-assisted solvothermal method in low temperature and short time synthesis (1 min). The PL measurements indicate an intense green light emission in capped ZnS and a less intense blue light emission in uncapped ZnS. The PL results can be attributed to distortions in the materials lattice. The different electronic levels appearing in the bandgap of capped and uncapped ZnS are able to create different colors emissions in the visible spectra of light. This effect was confirmed by first-principles calculations based on the B3LYP density functional theory using disorder models of the lattice.

ACKNOWLEDGMENTS

This work is supported by the Brazilian Funding Agencies FAPESP, CAPES, CNPq, and CEPID. We thank Ricardo Gonçalvez and Rorivaldo Camargo for their help with the FEG-TEM and FEG-SEM images. The computational research supported by resources supplied by Laboratório de Simulação Molecular and the Center for Scientific Computing of the São Paulo State University are also acknowledged.

[1]M. V. Limaye, S. Gokhale, S. A. Acharya, and S. K. Kulkarni, Nanotechnology **19**, (2008).
[2]S. Biswas and S. Kar, Nanotechnology **19**, (2008).
[3]M. Bredol and J. Merikhi, J. Mater. Sci. **33**, 471 (1998).
[4]P. Calandra, M. Goffredi, and V. T. Liveri, Colloids Surf., A **160**, 9 (1999).
[5]T. Yamamoto, S. Kishimoto, and S. Iida, Physica B **308**, 916 (2001).
[6]A. P. Alivisatos, Science **271**, 933 (1996).
[7]Z. F. Ding, B. M. Quinn, S. K. Haram, L. E. Pell, B. A. Korgel, and A. J. Bard, Science **296**, 1293 (2002).
[8]S. L. Lin, N. Pradhan, Y. J. Wang, and X. G. Peng, Nano Lett. **4**, 2261 (2004).
[9]W. Z. Wang, I. Germanenko, and M. S. El-Shall, Chem. Mater. **14**, 3028 (2002).
[10]H. F. Shao, X. F. Qian, and Z. K. Zhu, J. Solid State Chem. **178**, 3522 (2005).
[11]H. J. Liu, Y. H. Ni, M. Han, Q. Liu, Z. Xu, J. N. Hong, and X. Ma, Nanotechnology **16**, 2908 (2005).
[12]L. Chai, J. Du, S. Xiong, H. Li, Y. Zhu, and Y. Qian, J. Phys. Chem. C **111**, 12658 (2007).
[13]J. Y. Liu, Z. Guo, Y. Jia, F. L. Meng, T. Luo, and J. H. Liu, J. Cryst. Growth **311**, 1423 (2009).
[14]Y. W. Zhao, Y. Zhang, H. Zhu, G. C. Hadjipianayis, and J. Q. Xiao, J. Am. Chem. Soc. **126**, 6874 (2004).
[15]M. Sharma, S. Kumar, and O. P. Pandey, J. Nanopart. Res. **12**, 2655 (2010).
[16]Motlan, G. Zhu, K. Drozdowicz-Tomsia, K. McBean, M. R. Phillips, and E. M. Goldys, Opt. Mater. **29**, 1579 (2007).
[17]Y. Azizian-Kalandaragh and A. Khodayari, Phys. Status Solidi A **207**, 2144 (2010).
[18]J. Geng, B. Liu, L. Xu, F.-N. Hu, and J.-J. Zhu, Langmuir **23**, 10286 (2007).
[19]W. H. Zhang, J. L. Shi, H. R. Chen, Z. L. Hua, and D. S. Yan, Chem. Mater. **13**, 648 (2001).
[20]S. K. Maji, N. Mukherjee, A. Mondal, B. Adhikary, B. Karmakar, and S. Dutta, Inorg. Chim. Acta **371**, 20 (2011).
[21]W. G. Becker and A. J. Bard, J. Phys. Chem. **87**, 4888 (1983).
[22]K. J. Rao, B. Vaidhyanathan, M. Ganguli, and P. A. Ramakrishnan, Chem. Mater. **11**, 882 (1999).
[23]D. P. Volanti, D. Keyson, L. S. Cavalcante, A. Z. Simoes, M. R. Joya, E. Longo, J. A. Varela, P. S. Pizani, and A. G. Souza, J. Alloys Compd. **459**, 537 (2008).
[24]S. Komarneni, R. Roy, and Q. H. Li, Mater. Res. Bull. **27**, 1393 (1992).
[25]C. T. Lee, W. T. Yang, and R. G. Parr, Phys. Rev. B **37**, 785 (1988).
[26]R. Dovesi, V. R. Saunders, C. Roetti, R. Orlando, C. M. Zicovich-Wilson, F. Pascale, B. Civalleri, K. Doll, N. M. Harrison, I. J. Bush, P. D'Arco, M. Llunell, CRYSTAL06 User's Manual (University of Torino, Torino), 2006.
[27]R. C. Lima, L. R. Macario, J. W. M. Espinosa, V. M. Longo, R. Erlo, N. L. Marana, J. R. Sambrano, M. L. dos Santos, A. P. Moura, P. S. Pizani, J. Andres, E. Longo, and J. A. Varela, J. Phys. Chem. A **112**, 8970 (2008).
[28]M. L. Moreira, P. G. Cristianine Buzolin, V. M. Longo, N. H. Nicoleti, J. R. Sambrano, M. S. Li, J. A. Varela, and E. Longo, J. Phys. Chem. A **115**, 4482 (2011).
[29]N. L. Marana, V. M. Longo, E. Longo, J. B. L. Martins, and J. R. Sambrano, J. Phys. Chem. A **112**, 8958 (2008).
[30]L. S. Cavalcante, J. C. Sczancoski, V. M. Longo, F. S. De Vicente, J. R. Sambrano, A. T. de Figueiredo, C. J. Dalmaschio, M. S. Li, J. A. Varela, and E. Longo, Opt. Commun. **281**, 3715 (2008).
[31]J. E. Jaffe and A. C. Hess, Phys. Rev. B **48**, 7903 (1993).
[32]A. Lichanot, E. Apra, and R. Dovesi, Phys. Status Solidi B **177**, 157 (1993).
[33]M. J. D. Powell, SIAM Rev. **12**, 79 (1970).
[34]H. Z. Zhang, B. Gilbert, F. Huang, and J. F. Banfield, Nature (London) **424**, 1025 (2003).
[35]See http://www.crystal.unito.it/Basis-Sets for the site where you can get the basis of atoms to perform calculation/simulation, at the program crystal.
[36]E. H. K. a. M. M. Elcombe, Acta Crystallogr. C **39**, 1493 (1983).
[37]L. A. H. Klug, *X-Ray Diffraction Procedures* (John Wiley and Sons, Inc., New York, 1962).
[38]D. L. Wood and J. Tauc, Phys. Rev. B **5**, 3144 (1972).
[39]P. K. Ghosh, S. Jana, S. Nandy, and K. K. Chattopadhyay, Mater. Res. Bull. **42**, 505 (2007).
[40]P. H. Kasai and Y. Otomo, J. Chem. Phys. **37**, 1263 (1962).
[41]I. Uchida, J. Phys. Soc. Jpn. **19**, 670 (1964).
[42]N. Murase, R. Jagannathan, Y. Kanematsu, M. Watanabe, A. Kurita, K. Hirata, T. Yazawa, and T. Kushida, J. Phys. Chem. B **103**, 754 (1999).
[43]H. Chen, Y. Hu, and X. Zeng, J. Mater. Sci. **46**, 2715 (2011).
[44]Y. C. Li, X. H. Li, C. H. Yang, and Y. F. Li, J. Phys. Chem. B **108**, 16002 (2004).
[45]E. Longo, E. Orhan, F. M. Pontes, C. D. Pinheiro, E. R. Leite, J. A. Varela, P. S. Pizani, T. M. Boschi, F. Lanciotti, A. Beltran, and J. Andres, Phys. Rev. B **69**, 125115 (2004).
[46]V. M. Longo, L. S. Cavalcante, M. G. S. Costa, M. L. Moreira, A. T. de Figueiredo, J. Andres, J. A. Varela, and E. Longo, Theor. Chem. Acc. **124**, 385 (2009).
[47]M. Salavati-Niasari, M. R. Loghman-Estarki, and F. Davar, J. Alloys Compd. **475**, 782 (2009).
[48]L. Zhang and L. Yang, Cryst. Res. Technol. **43**, 1022 (2008).
[49]C. Cheng, G. Xu, H. Zhang, J. Cao, P. Jiao, and X. Wang, Mater. Lett. **60**, 3561 (2006).
[50]S. K. Panda and S. Chaudhuri, J. Colloid Interface Sci. **313**, 338 (2007).
[51]J.-Q. Sun, X.-P. Shen, K.-M. Chen, Q. Liu, and W. Liu, Solid State Commun. **147**, 501 (2008).